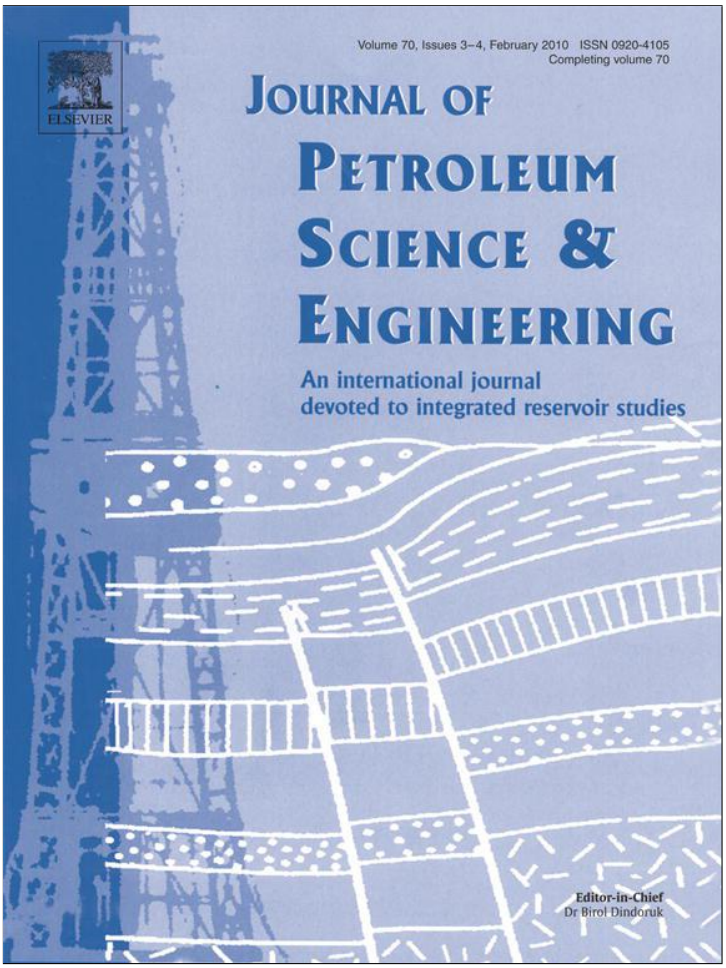

Journal of Petroleum Science and Engineering 70 (2010) 168–176

Contents lists available at ScienceDirect

Journal of Petroleum Science and Engineering

journal homepage: www.elsevier.com/locate/petrol

LDA and PIV characterization of the flow in a hydrocyclone without an air-core

L.P.M. Marins [a], D.G. Duarte [b], J.B.R. Loureiro [b,c,*], C.A.C. Moraes [a], A.P. Silva Freire [b]

[a] Petrobras Research Center (Cenpes/PETROBRAS), Rio de Janeiro, Brazil
[b] Mechanical Engineering Program (PEM/COPPE/UFRJ), C.P. 68503, 21945-970, Rio de Janeiro, Brazil
[c] Scientific Division, Brazilian National Institute of Metrology (DIMCI/INMETRO), 22050-050, Rio de Janeiro, Brazil

ARTICLE INFO

Article history:
Received 18 August 2008
Accepted 11 November 2009

Keywords:
hydrocyclone
LDA
PIV

ABSTRACT

The three-dimensional flow in a hydrocyclone especially developed for application in the petroleum industry has been investigated through the LDA and PIV techniques for one experimental condition. In the present physical simulation, the hydrocyclone is set to operate without an air-core. The tangential (V_θ) and axial (V_z) mean velocity profiles are analyzed through both measuring techniques. Radial (V_r) mean velocity profiles are only accounted for through PIV. The exponent n in the tangential velocity equation, $V_\theta r^n = C$, was determined to be about 0.61. For the radial profile, $V_r r^m = -D$, m was found to be 1.59. The rms-values of two-velocity components — tangential and axial — were evaluated via LDA. Turbulence in the axial direction is observed to be slightly higher than turbulence in the tangential direction. Approaching the axis of symmetry of the cyclone, however, this trend is reversed. The fluctuations in the tangential direction are found to be at least twice higher than the axial fluctuations.

1. Introduction

Devices that resort to centrifugal effects as a means to achieve phase separation in fluid systems are commonplace in industry. Despite their popular appeal, any comprehensive analysis on the physical and mathematical aspects of the problem is hampered by inherent difficulties related to the great variety of forms that are found in technology and to the very complex dynamics of the flow.

In fact, the fundamental idea behind a centrifugal separator is very simple. A swirling flow is produced which causes the heavier fluid or particle to be displaced outwardly. Then, specific strategies can be worked out to separate the distinct phases through different outlets. Depending on the aimed application, centrifugal separators may have to be loaded with solid particles, gases or liquids, at different relative concentration rates. Hence, geometry and operating conditions need to be carefully chosen so as to assure the best possible performance. Practical requirements may, for example, require the use of active or passive devices. Typical examples are, respectively, centrifugals and cyclones.

The qualitative description of swirling turbulent flows is a naturally complex problem. When the continuous phase is further loaded with a disperse phase the complexity of the problem is much aggravated for the interrelations between the two phases need to be adequately modeled. Thus, it is not a surprise to find that most design and operational issues rely on empirical equations. Of course, ad hoc experiments lead necessarily to models of a limited scope: the set of conditions to which the experiments were performed. An obvious and undesired consequence is that any extrapolation of results to a different geometry or operating condition has to be made with extreme caution.

The development of predictive mathematical models for the description of the flow within a centrifugal separator is thus a subject of utmost importance. Some early results based on the equilibrium orbit theory (Driessen, 1951) and the residence time theory (Rietema, 1961) helped to form much of the understanding we have today about centrifugal separators. However, it is undeniable that the recent advances in computational fluid dynamics (CFD) have offered alternative ways to the design of efficient separators that have become very attractive in terms of cost reduction and time saving. Important contributions are the recent works of Narasimha et al. (2006), Udaya Bhaskar et al. (2007) and Murphy et al. (2007).

The apparent more fundamental treatment of the flow in a centrifugal separator through CFD is, however, not free of difficulties. For instance, important questions related to the formation and stability of air-cores, the introduction of anisotropy and strain in turbulence or the interaction between distinct phases, need to be dealt with by suitable models. The implication is that any advanced methodology must be subjected to a thorough validation with rigorous experimental data.

One important purpose of the present work is to develop a reference experimental data base for the analysis of a particular type of hydrocyclone, especially developed for use in the petroleum industry. Laser-Doppler anemometry (LDA) and particle image velocimetry (PIV) are used to characterize the three-dimensional flow fields at six axial planes. In the present contribution, the hydrocyclone operates without

* Corresponding author. Mechanical Engineering Program (PEM/COPPE/UFRJ), C.P. 68503, 21945-970, Rio de Janeiro, Brazil.
E-mail address: jbrloureiro@gmail.com (J.B.R. Loureiro).

0920-4105/$ – see front matter © 2009 Elsevier B.V. All rights reserved.
doi:10.1016/j.petrol.2009.11.006

an air-core. Results for the mean and turbulent velocity fields are presented. The work also analyzes the dependency of the tangential and radial components of velocity on the radius of the hydrocyclone.

A conical hydrocyclone is a device with no moving parts. The swirling flow is naturally provoked by the tangential injection of inlet flow in a cylindrical chamber that is immediately followed by a conical section. Two outlet passages are commonly used in a hydrocyclone. The highest density fluid that is displaced to the outside of the wall is made to escape through a passage located opposite to the inlet and is called the underflow. The lowest density fluid moves to the center of the cyclone and escapes through an opening centered in the top of the inlet cylinder, the overflow. In the present hydrocyclone configuration, a vortex finder is not used. This is an important feature of hydrocyclones intended at removing oil from water or vice-versa. The inlet region of an oil–water separator must be such as to minimize the break up of droplets. With this in view, the development of smooth inlet regions, deprived of geometric features prone to induce regions with high shearing rates, flow deceleration and secondary circulatory flows is of extreme importance. The geometric arrangement of the hydrocyclone to be presently tested is shown in Fig. 1. The inlet section is, in fact, composed of two sections: a cylindrical inlet chamber and a section with cone angle of 15°. This assembly results in a gradual flow acceleration, with less pressure drop and turbulence production. A frustum with a cone angle of 1° is then connected to the inlet sections. Since in an oil–water separator the difference in densities of the working fluids is small, the residence time needs to be maximized. That is the reason for the adoption of a small angle in the present hydrocyclone.

Most laboratory studies have been concerned with the impact that changes on the operating conditions or geometry may have on the performance of hydrocyclones. Very few articles investigate the local mean and turbulent flow fields. This work expects to help fill this gap by studying thoroughly one type of hydrocyclone of great industrial appeal through two different experimental techniques. To the present authors' knowledge, this is the first time that LDA and PIV techniques are combined to offer a quantitative view on the flow in a hydrocyclone. In fact, some previous works (Fisher and Flack, 2002; Bergstrom and Vomhoff, 2007) have emphasized how difficult it is to make measurements in a hydrocyclone. For this reason, the use of redundant measurements to characterize the flow quantities is particularly important.

2. Experiments

2.1. Facilities, cyclone geometry

The experiments were carried out in a full-scale hydrocyclone entirely constructed of plexiglass and with the dimensions shown in Fig. 1. The service rig consisted basically of a 3000 l reservoir and a volumetric pump with top flow rate of 10 m^3/h and working head of 10 kgf/cm^2 at 1160 rpm. A set of valves was used to control the inlet flow rate through a 25.4 mm diameter pipe. A rotameter and a mini-LDV system were used to monitor the flow rate to within 0.1 m^3/h uncertainty. Three pressure transducers were used to measure the pressure in the inlet and outlet passages. The rig setup is illustrated in Fig. 2. The test conditions are shown in Table (1).

Measurements were conducted at eleven axial planes. Results are presented for the six selected positions shown in Fig. 3. Note the origin of the coordinate system.

2.2. Instrumentation

2.2.1. LDA system

A two-component TSI laser-Doppler anemometry system using a 5 W Ar-ion tube laser was operated in the backscatter mode to measure mean and fluctuating profiles of the tangential (V_θ) and axial (V_z) velocity components. A Bragg cell unit was used to introduce an optical–electronic shift of 10 MHz. That was necessary to resolve the direction of the flow field and give correct measurements of near-zero mean velocities. The beams were made to pass through a series of conditioning optical elements to achieve a small measurement

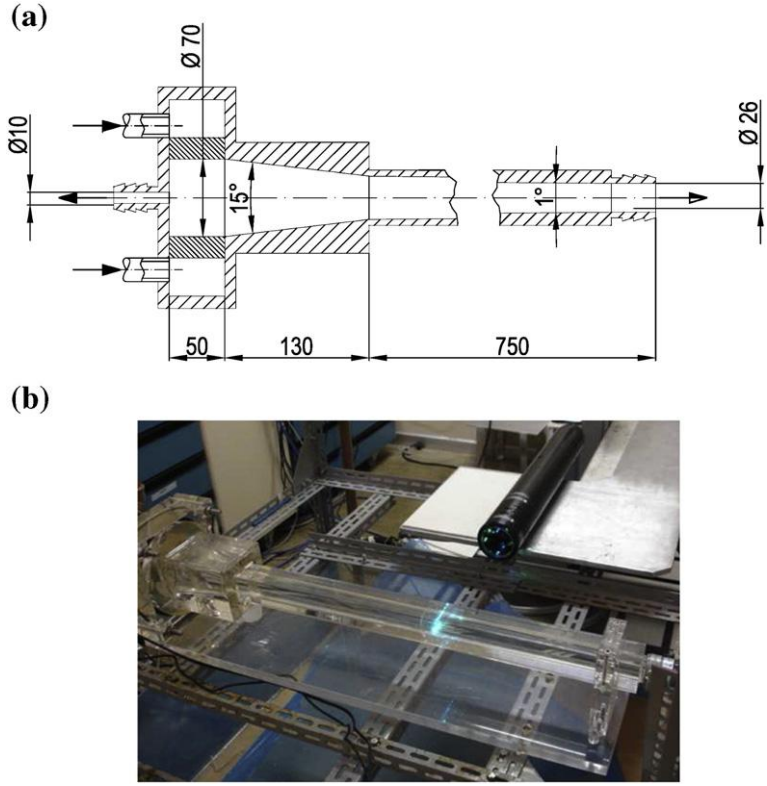

Fig. 1. Geometry of the hydrocyclone. Dimensions are in mm.

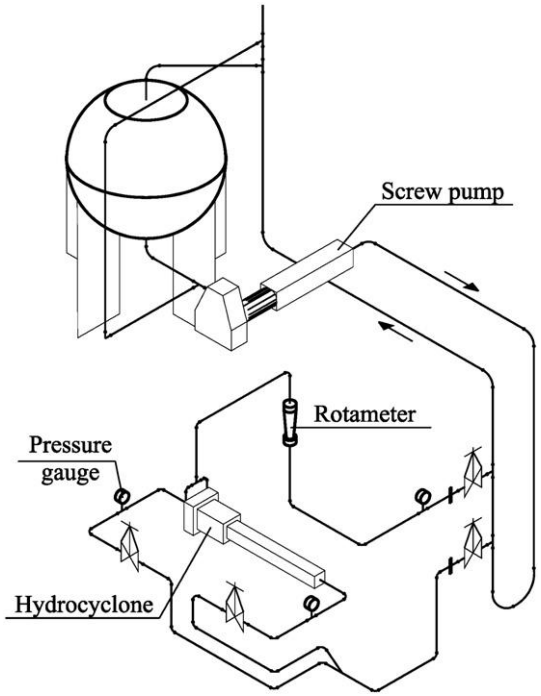

Fig. 2. Illustration of experimental setup.

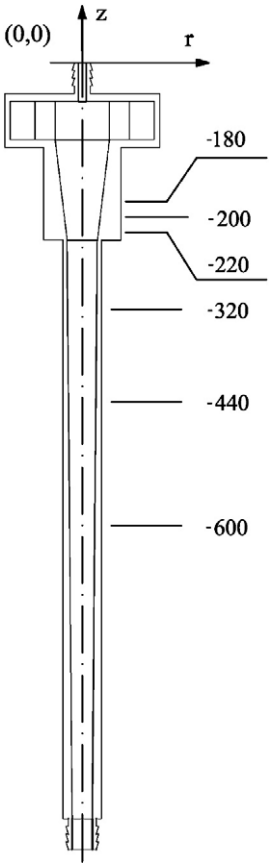

Fig. 3. Location of measuring positions and coordinate system.

volume and to improve the optical alignment. Front lenses with 260 mm focus length were mounted on the probe to accurately position the measurement volume. Before being collected by the photomultipliers, the scattered light was made to pass through interference filters of 514.5 nm and 488 nm, so that only the green and blue lights were received on each photomultiplier, respectively. Table (2) lists the main characteristics of the laser-Doppler system used. The signals from the photomultipliers were band-pass filtered and processed by a burst spectrum analyzer operating in a single measurement per burst mode. A series of LDA biases were avoided by adjusting the strictest parameters on the data processor. For the statistics at each point, 100,000 samples were considered.

To minimize the effects of reflection and refraction of the light beams, the external walls of the hydrocyclone (Fig. 1) were made flat. However, because the internal walls are conical in shape, the pairs of beams (green and blue) cross in different positions. This required the introduction of a physical model to correctly account for the actual position where the beams intersect. Typical uncertainties associated with the tangential (V_θ) and axial (V_z) mean velocity data are below 0.52% and 0.35% of the inlet mean velocity, respectively. Regarding the turbulent fluctuation components — $\langle v'_\theta v'_\theta \rangle^{1/2}$ and $\langle v'_z v'_z \rangle^{1/2}$ — uncertainties relative to the inlet mean velocity were estimated to be 0.36% and 0.25% respectively.

2.2.2. PIV system

The PIV measurements were performed with a Stereoscopic LaVision system. The light source was furnished by a double pulsed Nd:YAG laser that produced short duration (10 ns) high energy (120 mJ) pulses of green light (532 nm). The collimated laser beam was transmitted through a cylindrical (15 mm) and a spherical (500 mm) lens to generate a 1 mm thick lightsheet. The reflected light was recorded at 5 Hz by a CCD camera with 1280×1024 pixels and 12-bit resolution. The cameras were fitted with a Nikkor 105 mm f/2.8D lenses. The water was seeded with silver-coated glass particles, 10 μm in size. Image calibration was made by taking pictures of a reference target specially designed for the present purpose.

For all the measurements, the velocity vectors computational conditions were fixed. Adaptive correlation (DaVis 7.1 Software) has been processed on 32×32 pixel-size final interrogation spots, with 50% overlap, which gives a 64×64 vectors grid. The pixel resolution is 6.45×6.45 μm. Particle image treatment consists in using subpixel cell shifting and deformation, allowing bias and random error reduction. A widely accepted estimation of the absolute displacement error using these algorithms is 0.05 pixels. Different thresholds including signal-to-noise ratio and velocity vector magnitude were used as post-processing steps. Residual spurious vectors have been detected using a comparison with the local median of eight neighbour vectors for

Table 1
Experimental conditions.

Inlet flow rate	6.5 m^3/h
Inlet pressure	3.02 bar
Overflow pressure	1.20 bar
Underflow pressure	2.05 bar
Residence time	1.5 s
Reynolds number	89,500
DPR	1.87

Table 2
Main characteristics of the laser-Doppler system.

Colour	Green	Blue
Wavelength (nm)	514.5	488
Half-angle between beams	2.70°	2.56°
Fringe spacing (μm)	9.191	8.718
Beam diameter (mm)	2.2	2.2
Measurement volume		
Major axis (mm)	5.31	5.04
Minor axis (μm)	64.59	61.27

each grid points. No further filtering has been applied to the velocity fields in order to keep the whole measurement information.

3. Results

In the early experiments, a permanent concern was to visualize the flow field in a hydrocyclone. Results then suggested the flow to consist of two helical motions: an outer downward flow and an inner upward flow. The existence of a periodical motion at certain locations is sure to exert some influence on the measured quantities. In particular, the low mean radial velocities near the core of a hydrocyclone may be difficult to assess due to this phenomenon, the so-called precession of the vortex core.

Fig. 4 shows the instantaneous (18 μs) and the averaged (200 samples in 40 s) axial velocity fields in a section of the hydrocyclone. The precessing motion is clear. However, most of the reports on the behaviour of the velocity field of hydrocyclones present time-averaged results. Here, the same practice will be followed: mean profiles of the tangential, axial and radial velocity components are presented.

As mentioned before, measurements were made at eleven axial planes. In fact, tangential and axial velocity profiles were obtained in all eleven planes through LDA. Due to some geometric constraints, radial velocity profiles were not obtained via LDA. The geometric arrangement of the experiment also prevented PIV measurements to be made in the section of the cone with a 15° angle. The PIV data covers all three velocity components.

The typical behaviour of the tangential and axial mean velocity components is illustrated by the results at stations −180, −200, −220, −320, −440 and −600 mm (Figs. 5 and 6). The general agreement between the LDA and PIV data is very good. In particular, at positions −320 and −440 mm, the corresponding LDA and PIV data for V_θ and V_z

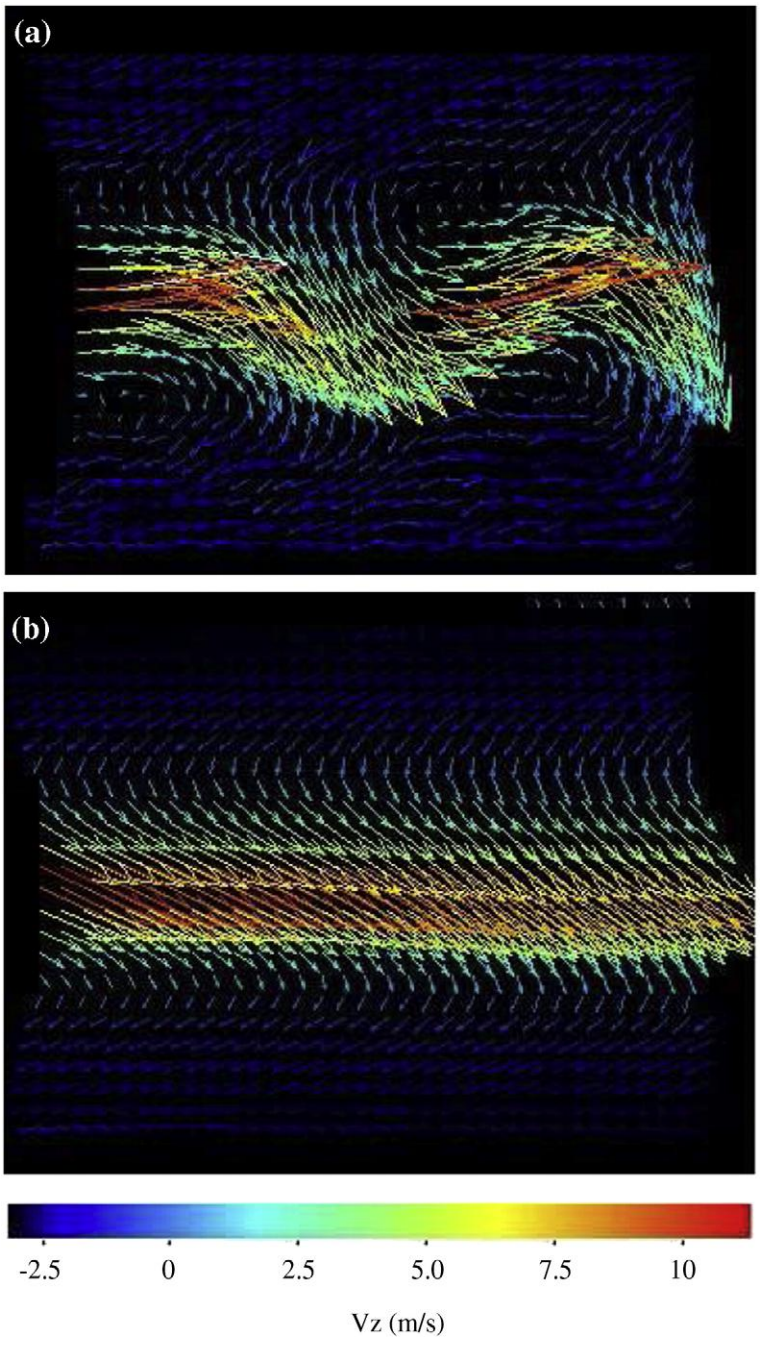

Fig. 4. The instantaneous and averaged velocity field in a hydrocyclone. a: Instantaneous profile; b: averaged profile.

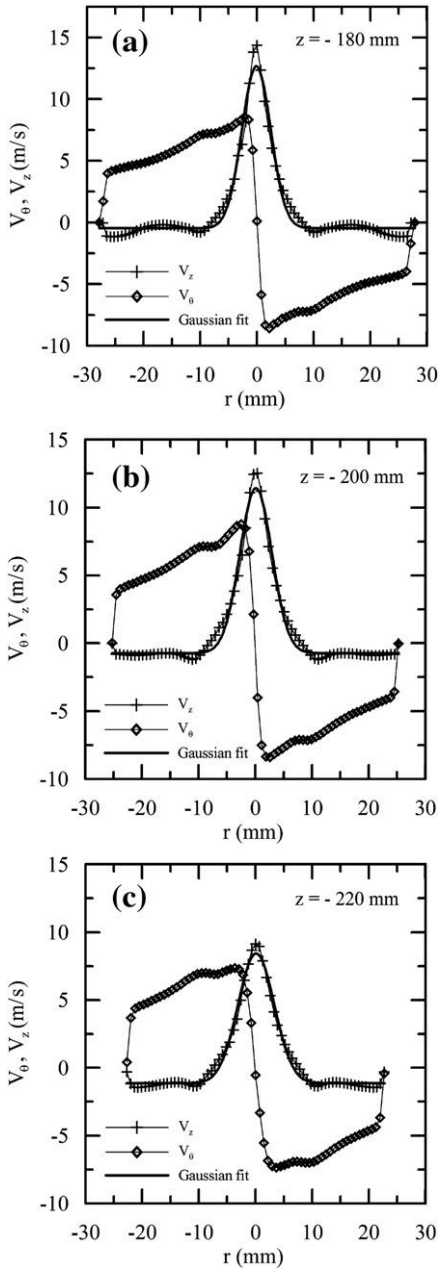

Fig. 5. Tangential and axial mean velocity profiles in the hydrocyclone section of 15° cone angle. LDA results. a: Position −180 mm; b: position −200mm; c: position −220 mm.

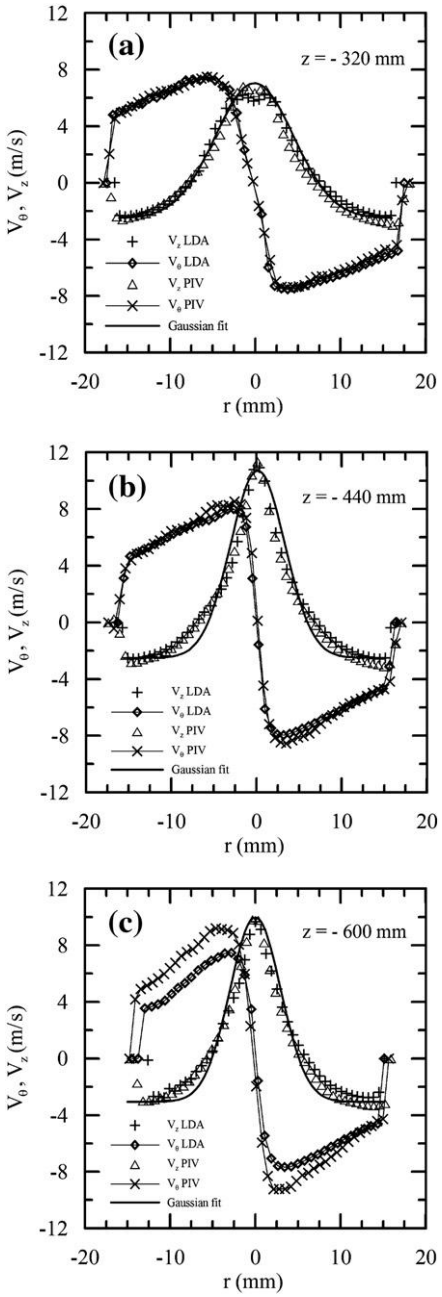

Fig. 6. Tangential and axial mean velocity profiles in the hydrocyclone section of 1° cone angle. LDA and PIV results. a: Position −320 mm; b: position −440 mm; c: position −600 mm.

agree almost exactly. Differences between measurements are mainly noted for the V_θ-profiles at position −600 mm. Table (3) compares measurements at the points of maximum velocity with the two techniques. For the V_z-profiles the highest relative difference is about 6%. For the V_θ-profiles, as much as 22% difference is observed.

The tangential mean velocity profiles — V_θ — follow the expected trend. They increase from the wall towards the center, reach a maximum and decrease rapidly to zero. Early studies (Kelsall, 1952) have divided the tangential profile in two parts: an inner part that closely resembles the rotation of a rigid body and an outer part that behaves like a free vortice with $V_\theta r^n =$ constant, and where V_θ is the tangential velocity, r the radius and n a parameter that varies between 0.84 and 0.75.

Yoshioka and Hotta (1955) found n to be 0.8 for a hydrocyclone with an air-core. Knowles et al. (1973) reports a value of n between 0.2 and 0.4 for a hydrocyclone operating without an air-core. These studies resorted respectively to a pitot-tube and cine photography to

Table 3
Comparison between LDA and PIV measurements.

Station	V_z (LDA) (m s^{-1})	V_z (PIV) (m s^{-1})	%
−320	6.21	6.60	5.91
−440	10.93	11.33	3.53
−600	9.66	9.76	1.02
Station	**V_θ (LDA) (m s^{-1})**	**V_θ (PIV) (m s^{-1})**	**%**
−320	7.35	7.46	1.47
−440	8.46	7.91	6.95
−600	9.22	7.58	21.64

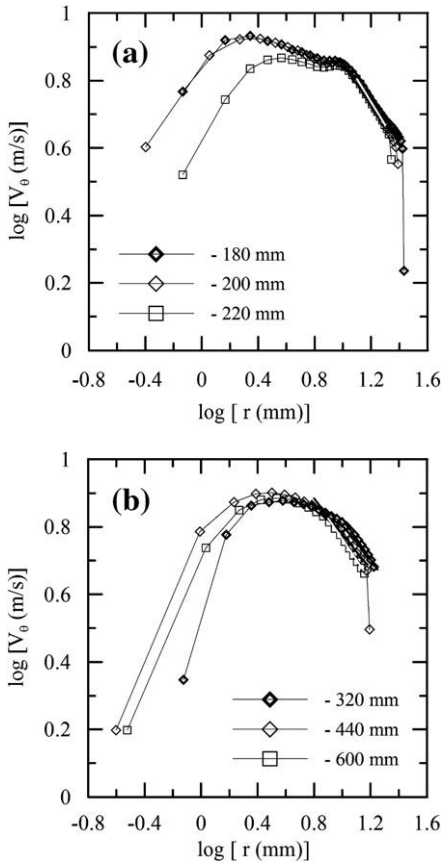

Fig. 7. Determination of the exponent n for the tangential mean velocity profiles in a hydrocyclone without an air-core ($V_\theta r^n = C$). LDA results. a: Positions −180, −200 and −220 mm; b: positions −320, −440 and −600 mm.

estimate the flow velocity. The more recent studies have shifted to laser-Doppler technique. Dabir and Petty (1986) investigated a hydrocyclone operated without an air-core; they found $n = 0.62$. Many other studies reached similar conclusion, including Morendon et al. (1992), Hwang et al (1993) and Chiné and Concha (2000).

The tangential mean velocity profiles for stations −320, −440 and −600 mm, plotted in bi-logarithmic coordinates are shown in Fig. 7. To each curve, a best straight line fit to the data is shown. The value of n is determined directly from the angular coefficient of the straight lines. Regarding the best curve fits, they were found by inspection of the coefficient of determination, R-squared (R_{sq}), defined by

$$R_{sq} = \frac{\Sigma_r}{\Sigma_e + \Sigma_r}, \quad (1)$$

where Σ_e is the residual sum of squares (sum of the squares of all the residual values) and Σ_r is the regression sum of squares (sum of squares of the differences between the average of all velocity values and the fitted velocity values at each radial or axial location where a data point occurs).

Table 4
Fitting statistics for the determination of n.

Station	n	Number of points used	R_{sq}
−180	0.612	7	0.999
−200	0.668	10	0.999
−220	0.678	10	0.999
−320	0.606	9	0.987
−440	0.524	11	0.976
−600	0.611	8	0.994

The coefficient of determination, R-squared shows how well the data are explained by the best-fit line (Bevington, 1969).

Table (4) shows the best fitting statistics, including the values of n. The present results are very close to the results of Dabir and Petty (1986) for the flow in a hydrocyclone operated without an air-core. For the six presented profiles, the average value of n is 0.617; Dabir and Petty (1986) found $n = 0.62$.

The axial mean velocity in a hydrocyclone is negative close to the wall and positive in the center. The negative sign denotes the flow that escapes through the underflow; positive velocity is related to the flow that leaves through the overflow. The velocity profiles in Figs. 5 and 6 are very nearly symmetric and detailed enough to characterize the boundary layer and the no-slip condition at the wall. All profiles follow a nearly Gaussian distribution (curves shown in the respective figures).

A Gaussian representation for V_z works very well for positions −180, −200 and −220 mm. However, in the 1°-cone, in particular at positions −440 and −600 mm, this pattern is not verified. In these two positions, the Gaussian distributions overestimate the underflow and overflow. Bearing this in mind, Table (5) shows the determined standard deviation (s) for the axial velocity profiles in Figs. 5 and 6. Typically, s increases in the 15°-cone, reaches a peak value at −320 mm (1°-cone) and then decreases.

In the present contribution, radial mean velocity profiles were only determined through PIV. Bergstrom and Vomhoff (2007) in their review paper show surprise with the fact that the radial velocity — V_r — is much less explored in literature as compared with the tangential and axial profiles. They further mention that this velocity component is probably the most important to understand the separation mechanisms. However, the few times that profiles are presented in the literature, they are difficult to interpret. They still argue that the radial velocity is much smaller than the other velocity components, what makes its assessment a difficult exercise.

Fig. 8 shows the radial mean velocity profiles for the present experiment in linear and bi-logarithmic coordinates. The inward (negative) velocity is largest close to wall, slowly decreasing as the centerline is approached. Very near the centerline, V_r passes through zero and becomes positive. The works of Kelsall (1952), Knowles et al. (1973) and Dabir and Petty (1986) were the first to report the behaviour of V_r. However, at the time, some important questions could not be settled since their radial velocity profiles were estimated from the other velocity components through continuity and axi-symmetry considerations. This practice naturally led to some contradictory results. Nonetheless, the results of Knowles et al. (1973) and Dabir and Petty (1986) suggest the values of V_r to be very low.

Direct measurements of V_r were presented by Luo et al. (1989), Chu and Chen (1993) and Fisher and Flack (2002). Luo et al. operated a hydrocyclone without an air-core. They used LDA to report exclusively inward radial velocities in the conical section. The radial velocity profile was also suggested to behave according to the expression $V_r r^m = -D$. Chu and Chen (1993) sustained the radial velocity to assume its maximum value close to the centerline. Fisher and Flack (2002) found the shapes and the magnitude of the radial velocity profiles to be essentially independent of the axial position.

Table 5
Standard deviation (s) for the axial velocity profiles shown in Figs. 5 and 6.

Station (mm)	s
−180	2.6
−200	2.8
−220	3.2
−320	4.6
−440	3.2
−600	3

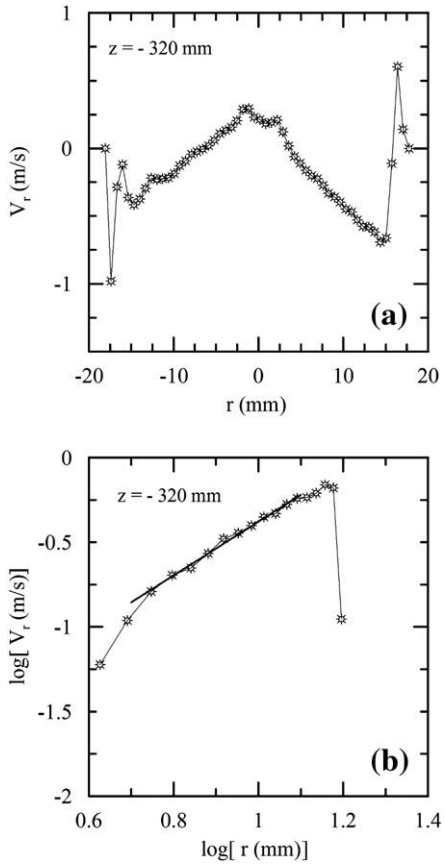

Fig. 8. Radial mean velocity profiles in a hydrocyclone without an air-core. PIV results. a: Linear plot; b: logarithmic plot.

The profiles were reported to approach zero for most of the domain, taking on a typical 2% of the mean tangential velocity. The present results show a maximum V_r close to origin and a profile that is nearly zero, about 2% of V_θ. The fitting procedure shown in Fig. 8b gives $m=1.59$. Luo et al. (1989) reported values of m ranging from 0.7 to 1.59.

Turbulence data are rarely presented for the flow inside a hydrocyclone. As the measuring volume is displaced inwardly, toward the centerline, optical noise resulting from the geometry and light attenuation decrease dramatically the data rate. This difficulty can be illustrated by Figs. 9 and 10. They show the time series of measurements taken at two distinct points in the axial plane −440 mm. The first point is located 11.9 mm away from the centerline, whereas the

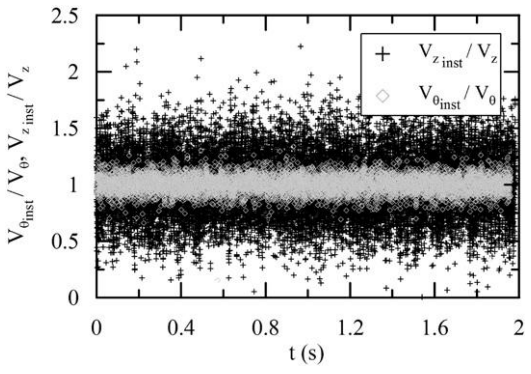

Fig. 9. Velocity sampling in a hydrocyclone without an air-core. LDA results. $z=-440$ mm, $r=11.9$ mm. In this figure $V_{z_{inst}}$ and $V_{\theta_{inst}}$ represent the instantaneous values of the axial and tangential velocity respectively.

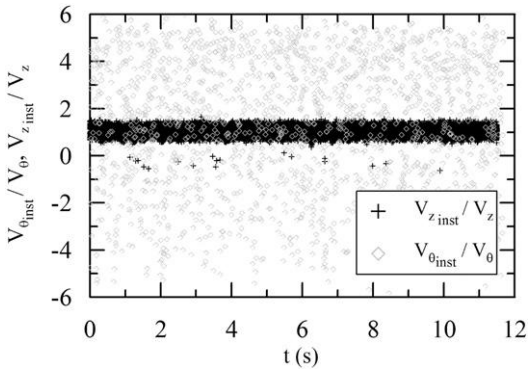

Fig. 10. Velocity sampling in a hydrocyclone without an air-core. LDA results. $z=440$ mm, $r=0.3$ mm. In this figure $V_{z_{inst}}$ and $V_{\theta_{inst}}$ represent the instantaneous values of the axial and tangential velocity respectively.

second point is detached 0.3 mm. At point #1 ($r=11.9$ mm), 73,500 samples were collected for the axial velocity and 28,250 for the tangential component, over 6.6 s. At point #2 ($r=0.3$ mm), 14 s were required to collect 32,761 and 2276 samples respectively for V_z and V_θ. The acquisition rates are then observed to vary between 11 and 0.16 kHz, depending on the flow position and velocity component.

The results show that at $r=11.9$ mm, the fluctuations in V_z and V_θ are of the order of 30% (for a 95% interval of confidence) and 10% respectively. At $r=0.3$ mm, these values change to 20% and 230% respectively. Please note that, at the centerline, V_z is at its maximum whereas V_θ is near-zero. Therefore, the root-mean square value of V_θ divided by its averaged value should give a very large value.

Despite the difficulties found in many points of the flow, acquisition rates of the order of 15 kHz were obtained in some other regions. The high sampling rates permitted the characterization of the tangential and axial turbulent profiles, the rms-values of V_z and V_θ.

In fact, the optical noise problem is further aggravated by the complexity of the flow. As the measuring volume approaches the geometric centerline of the hydrocyclone, the meandering of the flow makes the instantaneous two-velocity components in any axial plane difficult to distinguish. In a small vicinity of the symmetry axis, any instantaneous tangential velocity component can be mistaken with an orthogonal instantaneous radial velocity component. This is not a problem for the mean velocity components since positive and negative samples of both V_θ and V_r tend to cancel out to yield average values very near to zero at $r=0$. With the rms-values this does not happen.

In the following figures, we have used $v'_\perp$ to denote rms fluctuating quantities in an axial plane that are orthogonal to a given radial direction, $\vec{r}$. Thus, far away from the origin ($r\geq 0$) $v'_\perp \approx v'_\theta$. At the origin, $v'_\perp \approx v'_\theta + (v'_r)_\perp$, where $(v'_r)_\perp$ denotes the radial velocity fluctuations in a direction orthogonal to $\vec{r}$.

Fig. 11 shows the rms-values of v'_z and $v'_\perp$ at the axial planes −180, −200 and −220 mm. At position $z=-180$ mm the turbulence profiles still feel strongly the effects of the cylindrical inlet chamber. The axial component, $\langle v'_z v'_z\rangle^{1/2}$, presents a very distinct region of depression in the center. The rms profile of $V_\perp$ presents three distinct peaks of maximum velocity. At position −200 mm, the depressed turbulence axial component persists. However, the tangential component has already approached a Gaussian distribution. At the last position, −220 mm, both $\langle v'_\perp v'_\perp\rangle^{1/2}$ and $\langle v'_z v'_z\rangle^{1/2}$ profiles are nearly Gaussian. The general level of turbulence at the centerline always increases as z increases. This is true for both turbulence components. The near wall peaks in turbulence can be observed. The striking feature of Fig. 11 is, of course, the very high levels of turbulence present in the hydrocyclone.

In the region of 1°-cone angle, $\langle v'_z v'_z\rangle^{1/2}$ is shown (Fig. 12a) to be very sensitive to the changes in slope. At position $z=-320$ mm,

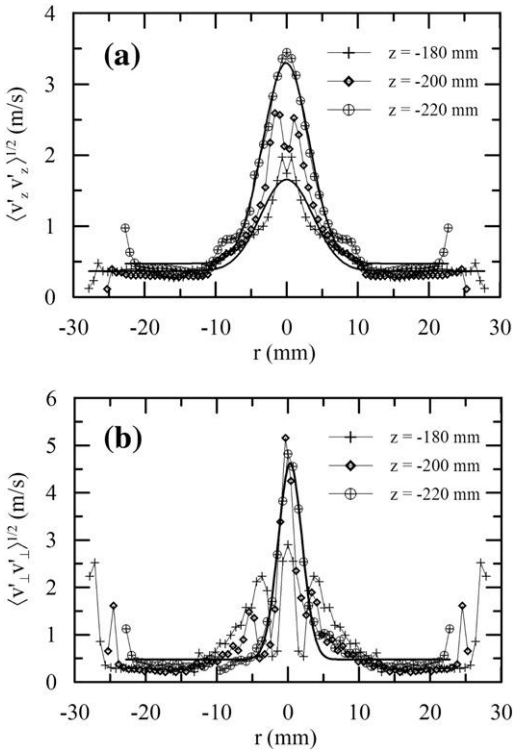

Fig. 11. Turbulence profiles in a hydrocyclone without an air-core. LDA results for positions −180 mm, −200 mm and −220 mm. a: $\langle v_z' v_z' \rangle^{1/2}$-profiles; b: $\langle v_\perp' v_\perp' \rangle^{1/2}$-profiles.

the $\langle v_z' v_z' \rangle^{1/2}$-profile shows a huge depression at the centerline. This behaviour is very pronounced and very well characterized. In opposition to the tendency previously observed in Fig. 11a, the levels of turbulence always decrease in Fig. 12a as z increases. In addition, the depression region accommodates to a Gaussian distribution.

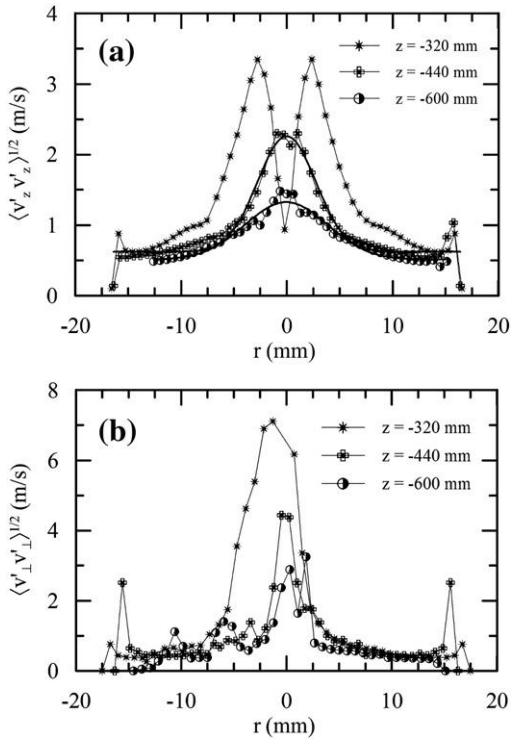

Fig. 12. Turbulence profiles in a hydrocyclone without an air-core. LDA results for positions −320 mm, −440 mm and −600. a: $\langle v_z' v_z' \rangle^{1/2}$-profiles; b: $\langle v_\perp' v_\perp' \rangle^{1/2}$-profiles.

Table 6
Local flow rates.

Station	Overflow (m^3h^{-1})	Underflow (m^3h^{-1})
−180	1.810	4.796
−200	1.956	5.325
−220	1.504	6.167
−320	1.548	4.206
−440	1.496	4.236
−600	1.064	4.651

The tangential turbulence component is shown in Fig. 12b. As z increases the peak values of $\langle v_\perp' v_\perp' \rangle^{1/2}$ always decrease.

The implication is that the two conical sections play very different roles in the flow properties as far as turbulence is concerned. The 15° conical section permanently increases turbulence whereas the 1° conical section does exactly the opposite.

The difficulties found in measuring the flow in a hydrocyclone are particularly illustrated in Table (6). The flow rates in Table (6) have been obtained from a direct integration of the local axial velocity profiles. Conservation of mass requires that, considered any two positions, the overflow of one position added to the underflow of the other position should equal each other. For most combinations, the mass balance is closed to within 10%. To some positions — −180, −320 and −440 mm — an accuracy of 5% is obtained. The sole particularly overestimated datum is 6.167 (position −220 mm).

4. Final remarks

The three-dimensional flow in a type of hydrocyclone aimed at applications in the petroleum industry has been characterized through the LDA and PIV techniques. All three components of the mean velocity profile have been characterized through LDA (two components) and PIV (all three components). The present data is judged accurate enough to serve as reference data for the validation of numerical simulations of the problem. In fact, the redundant measurement of the flow properties makes the present account of the problem very appealing.

Still in regard to model validation, the turbulence data should be of great help. We remind again the reader that turbulence data are very scarce in literature. For example, in one of the few exceptions, Chiné and Concha (2000) studied turbulence in a hydrocyclone using LDA. Most of the works currently under way, however, strive to develop computational models for the flow. The results introduced in Figs. 11 and 12 represent the state-of-the-art for turbulence measurements in hydrocyclones. For this reason, their importance cannot be overstated.

Acknowledgements

JBRL benefited from a Research Fellowship from the Brazilian Ministry of Science and Technology through Programme Prometro (Grant No 554391/2006-6). APSF is grateful to the Brazilian National Research Council (CNPq) for the award of a Research Fellowship (Grant No 306977/2006-0). The work was financially supported by the Brazilian Petroleum Company (Petrobras) through contract No PEM 6511. Further financial support was received from the Brazilian National Research Council (CNPq) through Grants No 477392/2006-7 and No 476091-2007/1, and from the Rio de Janeiro Research Foundation (FAPERJ) through Grants E-26/171.346/2005 and E-26/171.198/2003.

References

Bergstrom, J., Vomhoff, H., 2007. Experimental hydrocyclone flow field studies. Sep. Purif. Technol. 53, 8–20.
Bevington, P.R., 1969. Data Reduction and Error Analysis for the Physical Sciences. McGraw-Hill, NY.
Chiné, B., Concha, F., 2000. Flow patterns in conical and cylindrical hydrocyclones. Chem. Eng. J. 80, 267–273.

Chu, L.Y., Chen, W.M., 1993. Research on the motion of solid particles in a hydrocyclone. Sep. Sci. Technol. 10, 1875–1886.
Dabir, B., Petty, C., 1986. Measurement of mean velocity profiles in a hydrocyclone using laser Doppler anemometry. Chem. Eng. Commun. 48, 377–388.
Driessen, M.G., 1951. Theory of flow in a cyclone. Rev. L'Industrie Min. Spl. 267–273.
Fisher, M.J., Flack, R.D., 2002. Velocity distribution in a hydrocyclone separator. Exp. Fluids 32, 302–312.
Hwang, C.C., Shen, H.Q., Zhu, G., Khonsari, M.M., 1993. On the main flow pattern in hydrocyclones. J. Fluids Eng. 115, 21–25.
Kelsall, D.F., 1952. A study of the motion of solid particles in a hydraulic cyclone. Trans. Inst. Chem. Eng. 30, 87–108.
Knowles, S.R., Woods, D.R., Feuerstein, I.A., 1973. The velocity distribution within a hydrocyclone operating without an air-core. Can. J. Chem. Eng. 51, 263–271.
Luo, Q., Deng, C., Xu, J., Yu, L., Xiong, G., 1989. Comparison of the performance of water-sealed and commercial hydrocyclones. Int. J. Miner. Process. 25, 297–310.
Morendon, T.C., Hsieh, K.T., Rajamani, R.K., 1992. Fluid flow of the hydrocyclone: an investigation of device dimensions. Int. J. Miner. Process. 35, 68–83.
Murphy, S., Delfos, R., Pourquie, M.J.B.M., Olujic, Z., Jansens, P.J., Nieuwstadt, F.T.M., 2007. Prediction of strongly swirling flow within an axial hydrocyclone using two commercial CFD codes. Chem. Eng. Sci. 62, 1619–1635.
Narasimha, M., Brennan, M., Holtham, P.N., 2006. Large eddy simulation of hydrocyclone — prediction of air-core diameter and shape. Int. J. Miner. Process. 80, 1–14.
Rietema, K., 1961. Performance and design of hydrocyclones-1, 2, 3, 4. Chem. Eng. Sci. 15, 298–325.
Udaya Bhaskar, K., Rama, M.Y., Ravi, R.M., Tiwari, S., Srivastava, J.K., Ramakrishnan, N., 2007. CFD simulation and experimental validation studies on hydrocyclones. Min. Eng. 20, 60–71.
Yoshioka, N., Hotta, Y., 1955. Liquid cyclones as a hydraulic classifier. Chem. Eng. Jpn. 19, 633–641.